Na Channel Distribution in Vertebrate Skeletal Muscle

JOHN H. CALDWELL, DONALD T. CAMPBELL, and KURT G. BEAM

From the Department of Molecular and Cellular Biology, National Jewish Center for Immunology and Respiratory Medicine, Denver, Colorado 80206; the Department of Physiology, University of Colorado Medical School, Denver, Colorado 80262; and the Department of Physiology and Biophysics, University of Iowa School of Medicine, Iowa City, Iowa 52242

ABSTRACT The loose patch voltage clamp has been used to map Na current density along the length of snake and rat skeletal muscle fibers. Na currents have been recorded from (*a*) endplate membrane exposed by removal of the nerve terminal, (*b*) membrane near the endplate, (*c*) extrajunctional membrane far from both the endplate and the tendon, and (*d*) membrane near the tendon. Na current densities recorded directly on the endplate were extremely high, exceeding 400 mA/cm^2 in some patches. The membrane adjacent to the endplate has a current density about fivefold lower than that of the endplate, but about fivefold higher than the membrane 100–200 μm from the endplate. Small local variations in Na current density are recorded in extrajunctional membrane. A sharp decrease in Na current density occurs over the last few hundred micrometers from the tendon. We tested the ability of tetrodotoxin to block Na current in regions close to and far from the endplate and found no evidence for toxin-resistant channels in either region. There was also no obvious difference in the kinetics of Na current in the two regions. On the basis of the Na current densities measured with the loose patch clamp, we conclude that Na channels are abundant in the endplate and near-endplate membrane and are sparse close to the tendon. The current density at the endplate is two to three orders of magnitude higher than at the tendon.

INTRODUCTION

Essential to the functional organization of nearly every vertebrate cell is the nonuniform distribution of membrane proteins (Almers and Stirling, 1984). Characterizing these nonuniformities and elucidating the mechanisms that give rise to and maintain them are important steps toward an understanding of cellular and subcellular differentiation. Particularly striking examples of nonun-

Address reprint requests to Dr. John H. Caldwell, Dept. of Molecular and Cellular Biology, National Jewish Center for Immunology and Respiratory Medicine, 1400 Jackson St., Denver, CO 80206. Dr. Campbell's present address is Mark O. Hatfield Marine Science Center, Oregon State University, Newport, OR 97365. Dr. Beam's present address is Dept. of Physiology and Biophysics, Colorado State University, Fort Collins, CO 80523.

J. GEN. PHYSIOL. © The Rockefeller University Press · 0022-1295/86/06/0907/26$1.00

Volume 87 June 1986 907–932

iform distributions of membrane proteins are evident in the distribution of ionic channels in the membrane of neurons and muscle cells. Thus, in myelinated neurons, voltage-gated Na channels are concentrated both at the axon hillock (Catterall, 1981) and at the node of Ranvier (Conti et al., 1976; Ritchie and Rogart, 1977), whereas they are relatively sparse in internodal regions (Chiu and Ritchie, 1980) and possibly at the nerve terminal (Brigant and Mallart, 1982). In both neurons and muscle cells, the chemically gated channels mediating synaptic transmission are concentrated in the subsynaptic regions, near the sites of transmitter release. In skeletal muscle cells, indirect evidence suggests that Na channel density in the transverse tubular membrane may be lower than in the sarcolemma (Hille and Campbell, 1976; Jaimovitch et al., 1976).

This paper concerns the distribution of Na channels along the entire length of vertebrate skeletal muscle fibers. Our initial motive was to investigate the possibility that Na channel density was higher in the region of the endplate. Such a possibility had been suggested to account for the increased rate of rise of muscle action potentials near the endplate (Nastuk and Alexander, 1973; Thesleff et al., 1974), and had been strengthened by the observation that veratridine induced a steady inward current, which was blocked by tetrodotoxin (TTX), in the region of the endplate (Betz et al., 1984*b*). We used the loose patch voltage-clamp technique (Strickholm, 1961; Fishman, 1975; Stühmer and Almers, 1982) to determine the peak Na current density near the endplate of snake and rat muscle. We previously reported (Beam et al., 1985*a*, *b*) that Na channels are concentrated near the nerve terminal in both the obliquus externus abdominis muscle of the snake and the flexor digitorum brevis muscle of the rat. Roberts and Almers (1985) made similar observations in the costocutaneous muscle of the snake.

We have now extended these studies to all regions of the fiber, including the endplate itself and the region near the tendon. We describe a new preparation, the dissociated omohyoid muscle of the rat, which enabled us to make many of these measurements. In addition, we have tested the TTX sensitivity of Na current both close to and far from the nerve terminal.

We find that Na current densities are quite low near the tendon, moderate at midfiber regions between the tendon and the endplate, high near the endplate, and extremely high at the endplate. The parallel between this distribution of Na channels and the distribution of acetylcholine (ACh) receptor channels in skeletal muscle raises the possibility that similar mechanisms may be operating to concentrate both channel species near the endplate.

METHODS

Muscle Preparations

The experiments reported below were carried out with one of five different skeletal muscle preparations, two from the snake and three from the rat. Some muscles allowed us to record near the endplate but not the tendon, while the converse was true for others. These muscles were chosen primarily because they provided the visibility that allowed us to make the recordings reported here.

Snake. We first examined twitch fibers of the obliquus externus abdominis muscle

of the garter snake (*Thamnophis s. sirtalis*). A description of the anatomy of this muscle is given by Kuffler and Yoshikami (1975). Unlike frog skeletal muscle, the endplates of snake muscle are compact, like those in mammalian skeletal muscle. This endplate morphology, together with the ability to dissect the snake muscle to a thickness of a single fiber layer, makes it especially suitable for mapping studies. Twitch fibers were identified on the basis of their being singly innervated and larger than slow fibers. After being dissected free of other adhering muscles, the obliquus externus abdominis was pinned against the glass bottom of the recording chamber, using the skin and ribs as attachment points. In this muscle, it is simple to record near the endplate and anywhere up to several millimeters from the endplate, but not near the tendon.

To map near the tendon of snake muscle, we used a short (~1 mm) scale muscle close to the ventral midline. One end of the muscle inserts into the skin, and the other terminates in a sheet of connective tissue and is clearly visible (Fig. 6). Since this scale muscle is several fibers thick, measurements near the endplate were not feasible.

Rat. We used fibers of the flexor digitorum brevis (FDB) muscle of the rat. Individual fibers of this muscle are quite short (500–1,000 μm). The fibers were enzymatically dissociated using a modification of the procedure described by Bekoff and Betz (1977). FDB muscles were removed from 200-g male Sprague-Dawley rats and placed in a vial that contained "dissociation medium." The dissociation medium consisted of rat Ringer (described below) to which bovine serum albumin (1 mg/ml, fraction V) and collagenase (2 mg/ml, type 1) had been added (the albumin and collagenase were both from Sigma Chemical Co., St. Louis, MO). The vial containing the muscle was placed in a shaking water bath for 1–2 h at 37°C. During this time, the dissociation medium was continuously bubbled with oxygen. At the end of the 1–2-h period, the muscle was transferred from the vial to the experimental chamber containing physiological saline. Individual fibers were freed either by triturating the muscle with a fire-polished Pasteur pipette, or simply by repeatedly lifting the entire muscle in and out of the solution in the dish.

A fourth preparation that we used was enzymatically dissociated fibers of the rat omohyoid muscle. Compared with the FDB, fibers of the omohyoid are long (≥1 cm), which makes it necessary to adopt a different approach for enzymatic dissociation. For this purpose, the omohyoid muscle was placed in a small dish in which it was supported from below by fine nylon mesh. The dish was continuously perfused with oxygenated dissociation medium (composition described above) at a temperature of 30–32°C. After ~2 h, the muscle was transferred to the recording chamber containing rat Ringer. Individual fibers were freed by using a Pasteur pipette to direct gentle streams of solution against the surface of the muscle. Generally, it was relatively easy to free up the ends of fibers, but in the region of innervation the fibers were much more difficult to separate. Nonetheless, with practice it was possible to obtain a reasonably good yield of intact fibers (Fig. 7). It was only possible to record from dissociated muscle fibers that adhered to the bottom of the experimental chamber. In order to increase the percentage of adhering fibers, we found it helpful to clean the chamber with ethanol before use.

We used the intact omohyoid to map Na currents near the tendon. The muscle is shaped like a flat ribbon with fibers that run nearly parallel to the edges. Additionally, the omohyoid has a central tendon that perpendicularly transects some or all of the muscle. When this tendon extends to the edge of the muscle, single fibers at or near the edge can be studied both at the tendon and up to several millimeters away from the tendon.

Solutions

The physiological Ringer solutions contained (in millimolar with values given first for snake and then for rat): 145 or 146 NaCl, 4.3 or 5.0 KCl, 3.5 or 2 $CaCl_2$, 1.7 or 1 $MgCl_2$, 11 glucose, 10 HEPES, titrated with NaOH to pH 7.0 (snake) or 7.4 (rat).

When the effects of TTX were to be tested, the pipette was lifted off the surface of the muscle and the bathing solution was changed to one containing toxin. Suction was then applied to the pipette for a few minutes in order to load the tip with the toxin-containing solution. Suction was maintained during the approach of the pipette to the fiber surface and during the recording period. For recovery from toxin, the solution inside the electrode was replaced with toxin-free Ringer, and the toxin was washed out of the chamber.

Electrophysiological Procedures

Loose Patch Clamp. The experimental chamber was placed on the stage of an inverted microscope (Nikon Diaphot) equipped with Hoffman modulation contrast optics. Loose patch pipettes were fabricated from borosilicate-glass capillary tubing (5068, Rochester Scientific Co., Rochester, NY) with two separate pulls on a vertical puller (David Kopf Instruments, Tujunga, CA) and fire-polished to a final tip diameter of 2.5–20 μm. The pipettes were filled with ultra-filtered rat or snake Ringer as appropriate. Depending on the configuration of the taper and the tip diameter, the filled pipettes had resistances ranging from 100 to 700 kΩ. Before filling, the pipettes were bent at a point ~1.5 cm from the tip to nearly a right angle. The purpose of the bend was to allow the pipette tip to make a nearly perpendicular approach to the bottom of the recording chamber. The electrode was advanced slowly toward the surface of the muscle fiber with a piezoelectric positioner ("Inchworm," Burleigh Instruments, Fishers, NY), until the shunt resistance (i.e., the seal resistance separating the interior of the pipette from the bath) was about equal to the pipette resistance. Additional small advances of the pipette and the application of suction of 10–20 (isolated rat fibers) or 100–200 mmHg (snake muscle fibers and intact omohyoid) provided a further improvement in the shunt resistance and stability of the seal. The position of the pipette tip with respect to the endplate or tendon of a fiber was documented both photographically and by means of a television monitor. Current densities were calculated on the basis of the area of the orifice of the pipette tip. Thus, variations or surface irregularities in membrane area (e.g., T system or caveolae) could account for some of the variation in recorded current (see Discussion). Peak inward Na current densities have been expressed as positive numbers since we are concerned here primarily with the magnitude of the current.

The voltage-clamp circuit was that described by Stühmer et al. (1983). The bath potential was monitored with an FET-input operational amplifier (LF-356, National Semiconductor, Santa Clara, CA). A separate electrode was used for the current ground. After amplification and electronic filtration at 10–20 kHz with an eight-pole Bessel filter, the currents were digitized and stored for later analysis with a DECLAB 11/03 computer (Digital Equipment Corp., Maynard, MA). Although the voltage-clamp circuit provides electronic compensation for the bulk of the linear leakage and capacity current, it was still necessary to compensate digitally for the residual linear current by subtracting an appropriately scaled control current from the test currents. The standard sequence of pulses (given as depolarizations from the holding potential) was four control pulses (30 mV), test pulses in odd multiples of 7.5 mV (37.5, 52.5, 67.5, etc.), four more control pulses, and finally test pulses in even multiples of 7.5 mV (45, 60, 75, etc.). All experiments were carried out at temperatures of 20–22°C.

To determine patch-to-patch variation in Na current density, it is important that several criteria be satisfied. The first of these is that large changes in holding potential must not occur during the course of measurements on a single fiber since these changes can cause large variations in the measurement of peak Na current density. With the loose patch clamp, the absolute holding potential is a function of both the pipette potential and the

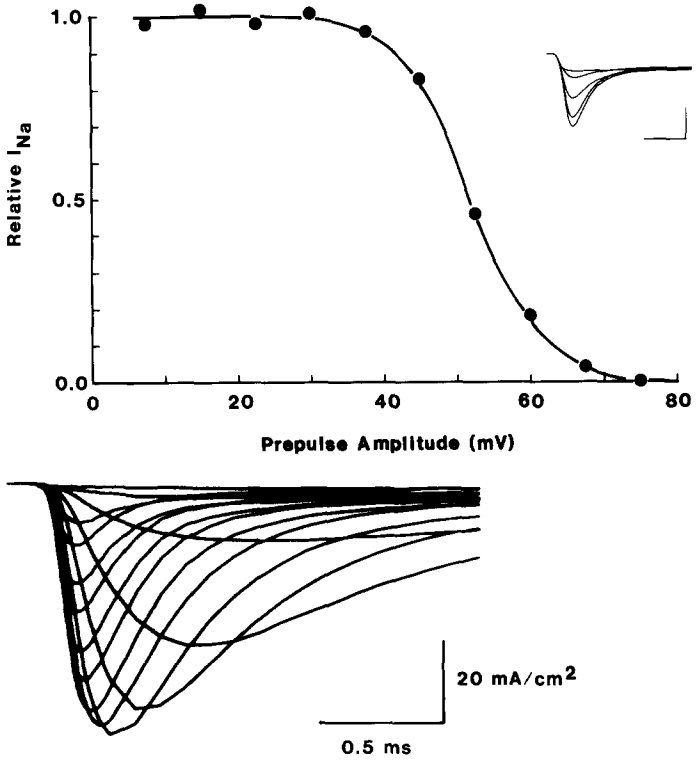

FIGURE 1. Estimation of holding potential and peak current density. (*A*) Steady state inactivation of Na current determined with a two-pulse protocol. The 40-ms conditioning prepulse to various potentials was followed by a constant test pulse of +120 mV (with respect to the holding potential). The inset shows the Na currents measured for prepulses varying in size from +37.5 (largest inward current) to +67.5 mV (smallest inward current), in 7.5-mV increments (the vertical calibration equals 20 mA/cm^2; the horizontal calibration equals 0.5 ms). The normalized current peaks vs. the prepulse amplitude are plotted. The curve represents a two-state Boltzmann distribution with a midpoint of 52 mV and an effective valence of 5.2. (*B*) Family of currents measured in the same fiber for test pulses of +60 to +157.5 mV from the holding potential in 7.5-mV increments. Intact rat omohyoid muscle; fiber 34-28; pipette diameter, 12 μm. For this fiber, the holding potential was calculated to be −128 mV, assuming that the midpoint of the steady state inactivation curve occurs at an absolute potential of −76 mV. Thus, the peak Na current in *B* was elicited by a test pulse to approximately −30 mV. The potentials given throughout the rest of the paper represent absolute potentials estimated in a similar manner.

fiber resting potential, and the latter is not explicitly measured. We therefore estimated the holding potential from the voltage dependence of the Na current. Periodically throughout an experiment, we determined the level of steady state inactivation as illustrated in Fig. 1*A*. The holding potential was estimated by assuming that half-inactivation occurred at −76 mV in the rat (Almers et al., 1984) and −75 mV in the snake. Furthermore, for each patch, the peak Na current was determined by measuring

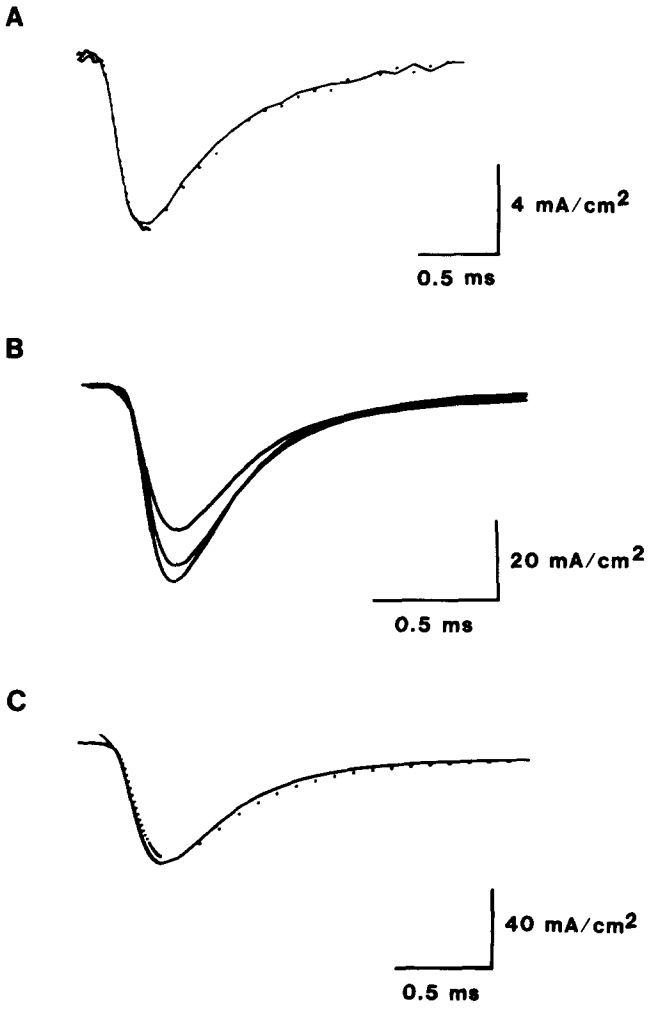

FIGURE 2. Three control experiments testing the reliability of measurements of current density. (*A*) Currents measured at the same test potential (−18 mV) for two successive placements of the pipette at the same site. Intact snake muscle; fiber 4-13. (*B*) Effect of the duration of a hyperpolarized holding potential on the peak Na current amplitude. The currents were recorded 1 (smallest), 3 (intermediate), and 5 (largest) min after applying a holding potential of −118 mV. Test potential, −13 mV. Intact omohyoid muscle; fiber 34-6. (*C*) Effect of increasing R_{shunt} on peak current. Currents were recorded at the same site with R_{shunt} equal to 190 (dots) and 280 (continuous trace) kΩ. $R_{pipette}$ was 120 kΩ. Same muscle fiber as in part *B*; test potential, −28 mV.

test currents for test pulses of varying amplitude (Fig. 1*B*). Thus, small shifts in the resting potential could also be detected by comparing individual current records for changes in the voltage dependence of activation and inactivation.

Another important criterion of reliability is that the measurement of current density at a particular site should be reproducible. An experimental test of reproducibility is

illustrated in Fig. 2*A*. Na currents were measured at a site on an intact snake muscle fiber. The pipette tip was then raised ~10 μm and placed back down on the identical site. As can be seen in the figure, the peak Na currents measured during two successive placements were virtually identical. A second important criterion for the patch-to-patch comparison of Na current density is that there be no appreciable variations in short- or long-term inactivation. This was not a significant problem for snake fibers, which typically have in vitro resting potentials of −90 to −100 mV. However, the rat muscle fibers (particularly the dissociated fibers) had low resting potentials that made it necessary to hyperpolarize the membrane considerably in order to obtain Na currents large enough for reliable measurement. Moreover, rat muscle shows a prominent slow component of inactivation (Almers et al., 1983*b*). Thus, for the rat muscle fibers, it was important to ensure that, before the measurement of test currents, all patches were held at a hyperpolarized potential long enough to achieve an equivalent removal of long-term inactivation. In practice, holding potentials of −100 to −130 mV (a single holding potential was used for a given fiber) were maintained for 2–4 min before test currents were recorded from a patch. Almers et al. (1983*b*, Fig. 8) observed that slow inactivation in the rat omohyoid has a time constant of ~2 min at 10°C and −90 mV. With higher temperatures (20–22°C in our experiments) and more negative holding potentials, the removal of slow inactivation is faster. Fig. 2*B* illustrates the Na currents measured from a single patch of an omohyoid muscle after various durations of holding at an estimated potential of −118 mV. The peak Na current after 1 min is already 72% of the value attained after 5 min. Thus, holding durations of 2–4 min should have been sufficient to remove most inactivation. Nonetheless, it seems likely that patch-to-patch variations in the removal of long-term inactivation have contributed some variability to our measurements of peak Na current density in the rat. A further control against unwanted contributions from long-term inactivation was our strategy of using two mapping sweeps along the fiber and having these sweeps cover overlapping portions of the fiber (see Results).

The currents illustrated in Fig. 2*B* (see also Fig. 12) are noteworthy because they are quite large compared with previous measurements of Na current density in rat muscle (Pappone, 1980; Almers et al., 1983*b*, 1984). Although we did not explore this point in greater detail, the large current densities appear to be a consequence of the fact that we held the potential 20–30 mV more negative than Pappone or Almers et al. did.

In mapping individual sites along the fiber, we attempted to achieve shunt resistances between the pipette and fiber surface that were about the same for all sites. Because some variations inevitably did occur, we examined the effect of changes in shunt resistance on the current measured at a single site. Fig. 2*C* compares the peak Na currents measured at the same site for shunt resistances of 190 and 280 kΩ. Increasing the shunt resistance by a factor of 1.47 produced a small change in current kinetics but almost no change in the amplitude of the peak current. From this and similar experiments, we concluded that the measurement of peak current was independent of shunt resistance, as long as the shunt resistance was at least 1.2 times the pipette resistance.

Vibrating Electrode

A vibrating microelectrode was used to measure extracellular current. The technique has been described in detail elsewhere (Jaffe and Nuccitelli, 1974; Betz and Caldwell, 1984). The method allows measurement of currents as small as 0.1 $\mu A/cm^2$, but to achieve this sensitivity the signal must be averaged for several seconds. Thus, it is useful for steady or slowly varying currents. In addition, the method does not provide the spatial resolution of the loose patch clamp. We induced a steady Na current with veratridine or veratrine (a mixture of alkaloids, one of which is veratridine). The muscles were pretreated with α-bungarotoxin to block currents created by the release of ACh from nerve terminals.

RESULTS

Distribution of Na Current Density in Snake Muscle

For our initial experiments, we chose to map Na current densities in fibers of the garter snake. The obliquus externus abdominis muscle was used to map Na current near the nerve terminal and in regions up to several millimeters from the nerve terminal. To map Na current close to the tendon, we used a short scale muscle from ventral-most skin; one tendon of this muscle ends in a thin sheet of connective tissue.

Near the endplate. A plot of Na current density vs. distance from the endplate in an intact snake muscle fiber is shown in Fig. 3. It is evident that the peak Na current density in snake skeletal muscle is high near the endplate and falls off rapidly with longitudinal distance away from the endplate. Table I gives the average current densities determined at near (within 35 μm), intermediate (between 35 and 250 μm), and far distances (>250 μm) from the endplate in 11

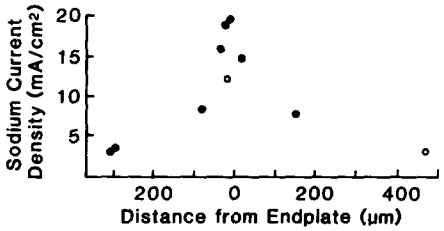

FIGURE 3. Peak inward Na current density as a function of longitudinal distance from the endplate in a snake muscle fiber. Fiber 4-1. The open circles are for measurements progressing from left to right and the solid circles are from subsequent measurements progressing from right to left. None of the measurements was made from sites overlapping the endplate.

snake fibers. The average inward current density from 20 near-endplate determinations was 18.1 mA/cm^2, 4.9 times the average density from 26 distal sites. Since the fall-off with distance is precipitous, these figures understate the extremely high densities found close to the endplate. Therefore, we also compared the highest density recorded near the endplate in a given fiber with the average distal density in the same fiber. The mean of the highest/distal ratio in seven fibers was 8.6 ± 3.2 (mean ± SD), with a range of 6.4–14.3. In an eighth fiber, this ratio was 1.9.

We also mapped the distribution of Na channels in two fibers where the endplate was on the edge of the fiber. In both cases, the current density fell quickly as the electrode was moved circumferentially away from the endplate. Fig. 4 shows Na current recorded at several positions in the vicinity of the endplate. It is clear that the Na current density is not elevated equally throughout the endplate segment of the fiber but rather that the endplate itself is the focal point of the increased current density.

Extrajunctional, far from the endplate. "Hot spots" of moderately increased Na current density have been reported previously in frog skeletal muscle by

Almers et al. (1983*a*). They found that the Na current density in some fibers varied as much as threefold over distances of 10–30 μm. They observed a much smaller variation in other fibers. Because the relationship between the measurement sites and the location of the endplate was undetermined in their study, we tested for the presence of similar variations in snake fibers at locations that we could visibly establish to be well away from the endplate. Fig. 5 shows a plot of peak current density from three representative fibers. Consistent with the observations of Almers et al. (1983*a*), we found up to a twofold variation in distances as short as 10–20 μm in the snake. However, in no case did we find "hot spots" with densities that approached those found in the region of the endplate.

Near the tendon. In two scale muscle fibers, the Na current density was mapped at the tendon (Fig. 6). In both fibers, the density decreased near the

TABLE I

Inward Na Current Densities Measured in Intact Snake Muscle

Fiber	$d < 35$ μm	$35 < d < 250$ μm	$d > 250$ μm	Highest near-endplate current
	mA/cm^2	mA/cm^2	mA/cm^2	mA/cm^2
4-1	23 (5)*	7.6 (7)	4.0 (4)	26.5
5-8	9.5 (3)		5.3 (1)	10.3
6-2	21.3 (4)	7.8 (9)	3.2 (7)	26.0
7-1	18.3 (2)		2.4 (2)	25.5
8-5	15.5 (2)		3.0 (2)	18.5
9-1		3.5 (1)		
10-1		5.0 (7)		
11-2	16.9 (1)			16.9
12-1	16.5 (1)			16.5
35-10	14.3 (1)		1.0 (1)	14.3
35-25	17.6 (1)		2.3 (1)	17.6
	18.1±6.1	7.7±5.0	3.7±1.3	19.1±5.7
	$n = 20$	$n = 16$	$n = 26$	$n = 9$

* The number of observations is given in parentheses. d = distance of the recording site from the nearest edge of the endplate.

tendon, falling threefold over the 200 μm closest to the tendon. A decrease in current density at the tendon was also observed in rat muscle (see below), where current densities were larger and easier to map.

Distribution of Na Current Density in Rat Muscle

We examined a number of different rat skeletal muscle preparations, including the sternothyroid, triangularis sterni, and omohyoid, to determine their suitability for mapping. Although all of these preparations are relatively thin, none was less than several fiber layers thick. Hence, although one could identify individual endplates, it was difficult to determine unambiguously the fiber innervated. Even when this determination was possible, the complex criss-crossing of fibers in the region of innervation made it difficult to follow the innervated fiber over a

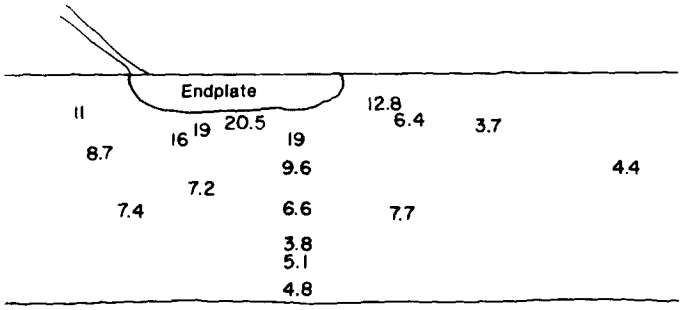

FIGURE 4. Circumferential decrease in peak Na current density. Snake obliquus externus abdominis fiber. The inward current density (mA/cm^2) is indicated at each recording position. The space constant for both the circumferential and longitudinal decrease in current density was shorter than for most snake fibers. The estimated resting potential was −90 mV and the fiber was held at this potential. Pipette diameter, 10 μm; fiber diameter, 80 μm; pipette resistance, 210 kΩ. Shunt resistances varied from 210 to 310 kΩ.

sufficient distance to permit us to determine the distribution of peak Na currents as in Fig. 3. We therefore chose to make measurements in enzymatically dissociated fibers of the rat FDB muscle, which has short (≤1 mm) fibers, and the rat omohyoid, which has fibers ~1 cm long.

Dissociated fibers. The endplate of rat muscle is a region defined by the branching of the motor nerve. The branches terminate in boutons beneath which the endplate membrane is thrown into synaptic (secondary) folds (Ishikawa et al., 1983). The tops of the synaptic folds contain densely packed ACh receptors (Fertuck and Salpeter, 1974). Between the boutons, the endplate is nonsynaptic and is free of folds and densely packed ACh receptors. As illustrated in Figs. 7 and 8, the dissociation process frequently results in fibers in which the presynaptic terminal has been dissociated free from the fiber surface. We found Na currents

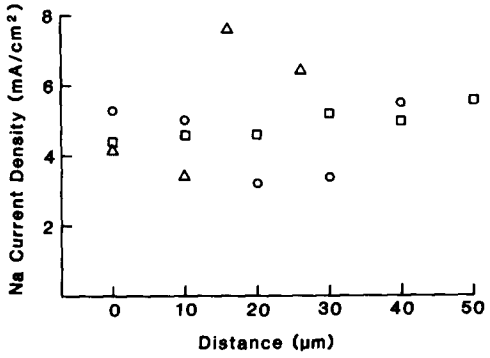

FIGURE 5. Short-range variation in peak inward Na current density measured midfiber in intact snake muscle. Distances are arbitrarily referred to the first recording site. All recording sites were >400 μm from the endplate and >1 mm from the tendon. Triangles: fiber 25-1; circles: fiber 25-7; squares: fiber 10-4.

to be largest when measured from the exposed endplate region. Recordings from 21 fibers, made with both large and small patch pipettes (see below), gave a current density of 139 ± 86 mA/cm^2 (mean ± SD). One of these fibers, together with the recording pipette, is shown in Fig. 8. The endplate region, as defined by fluorescent α-bungarotoxin binding, is shown in the inset and coincides with the area visualized as endplate with Hoffman modulation contrast optics. Fig. 9 illustrates Na currents recorded from an endplate and shows that they are about fivefold larger than currents recorded immediately adjacent to the endplate. The high Na current densities recorded at the endplate are not an artifact of the

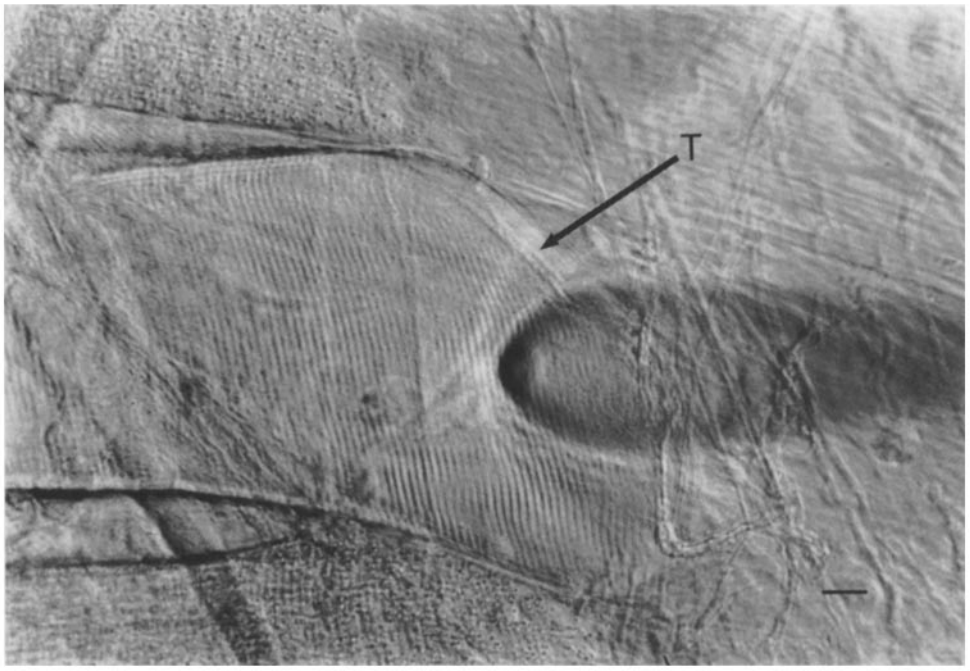

FIGURE 6. The tendon end (T) of an intact scale muscle from a snake. The shadow of the recording pipette extends over the connective tissue sheet in which the muscle terminates. Pipette tip diameter, 10 μm. Scale bar, 20 μm.

enzymatic dissociation, since currents of similar density have been recorded from snake muscle endplates that were exposed by denervation (Caldwell and Milton, 1985).

We used both large (15–20 μm) and small (2.5 μm) patch pipettes to record Na currents at the endplate. The average current density measured with large pipettes from endplates of six fibers was 76 ± 16 mA/cm^2. This value is lower than that measured with small pipettes (see below). There appear to be two reasons for this difference. First, the peak currents were sufficiently large (100–200 nA) with the large pipettes that the membrane patch escaped effective potential control. Thus, an intracellular electrode inserted 20 μm from a large patch pipette showed a 16-mV depolarization inside the fiber when the peak

inward Na current was 90 nA. Therefore, if voltage-clamp conditions are to be maintained at the endplate, small patch pipettes must be used. Additionally, since the large patch pipettes cover a significant fraction of the entire endplate, they record both from subsynaptic membrane and from membrane between nerve terminal boutons.

Na currents recorded from the endplate with 2.5-μm-diam pipettes can be >400 mA/cm^2 and can vary enormously within a single endplate. The endplates of three fibers were mapped in detail; one of these is shown in Fig. 10. The peak

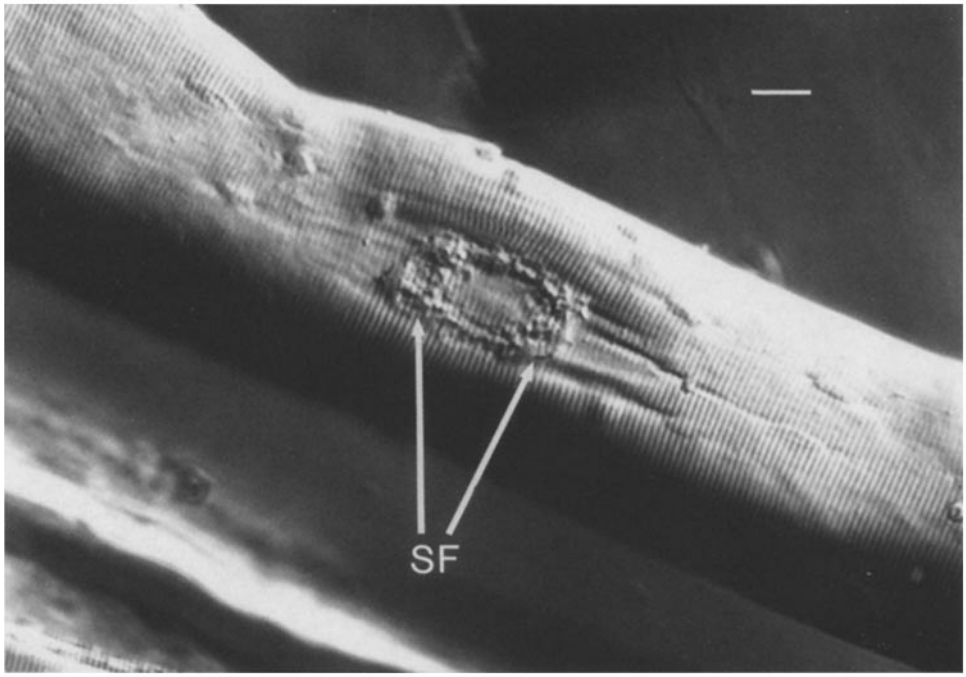

FIGURE 7. The exposed synaptic membrane of an enzymatically dissociated omohyoid muscle. Removal of the nerve terminal exposed an oval region of secondary folding (SF), which encloses a smooth central region that presumably has a low ACh receptor density. Scale bar, 20 μm.

inward currents in Fig. 10 range from <10 to >400 mA/cm^2. In the other two fibers, the currents ranged from <10 to 184 and from 51 to 245 mA/cm^2. The average current density for the 2.5-μm pipettes (excluding positions where Na current was <0.5 nA) was 169 ± 90 mA/cm^2 (mean ± SD, n = 14). It is unlikely that the low Na current density at some positions was due to variations in the shunt resistance since the shunt was 1–1.9 MΩ (pipette resistance, 680 kΩ), and there was no correlation between the size of the current and the various shunt resistances. It is also unlikely that the small currents were the result of damage since the measurement of large and small currents was unrelated to the sequence

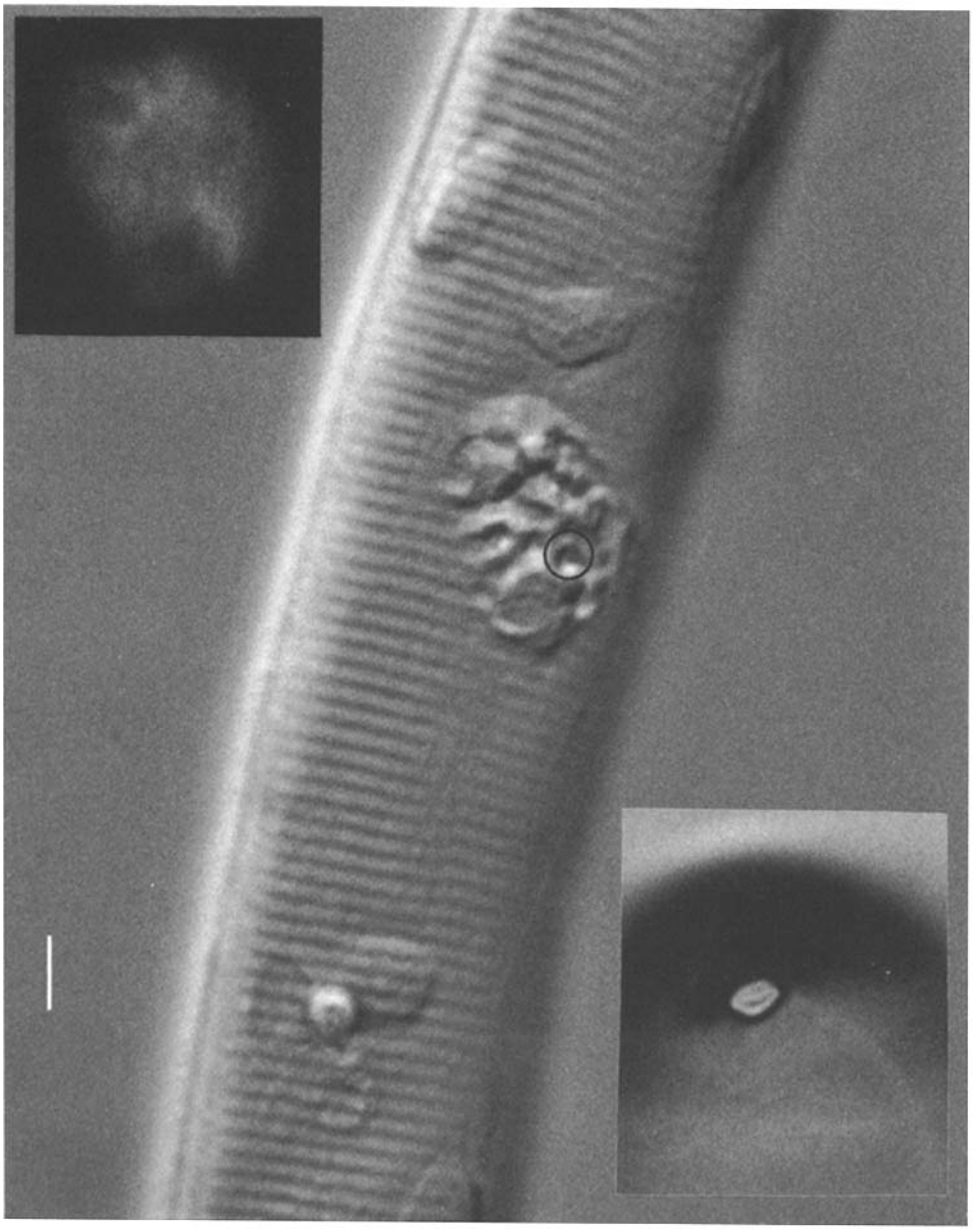

FIGURE 8. Endplate region of a single dissociated rat FDB fiber. The lower right inset shows the pipette tip and the upper left inset is a fluorescence micrograph of fluorescein isothiocyanate α-bungarotoxin (4 μg/ml), which was bound before recording from this endplate. The recording position is indicated by the black circle and contained both subsynaptic and nonsynaptic membrane. Peak Na current density from this spot was 126 mA/cm^2. Scale bar, 10 μm.

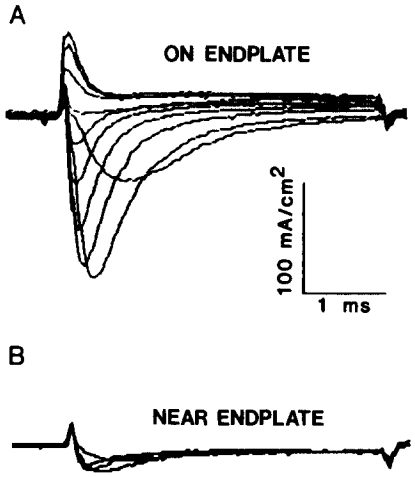

FIGURE 9. (*A*) Na currents recorded directly from endplate membrane of a dissociated rat FDB fiber. The nerve terminal was removed by enzymatic dissociation. The fiber was situated in the dish in such a way that the endplate was accessible to the pipette. Voltage steps were from −52 to +83 mV in 15-mV increments. (*B*) Currents recorded 5 μm from the border of the endplate. Voltage steps were from −52 to −7 mV in 15-mV increments. Holding potential, −112 mV; pipette diameter, 4 μm; pipette resistance, 600 kΩ; shunt resistance, 3.6 (*A*) and 3.7 (*B*) MΩ. Fiber 1127-5.

of recording. Unfortunately, we were not able to determine visually whether the pipette lay on or between regions of subsynaptic membrane. Possible explanations for these variations in Na current are discussed later.

Near the endplate. Na current densities near the endplate are high but considerably lower than at the endplate. Thus, the average peak inward current density from 13 FDB fibers at sites 5–15 μm from the endplate was 29.5 ± 12

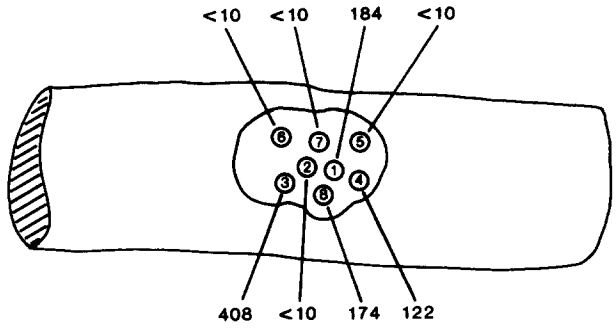

FIGURE 10. Peak inward Na current density recorded at eight positions within a single endplate of a dissociated rat FDB fiber. The numbers within the circles indicate the sequence of recording. The numbers above and below the fiber indicate the current density (mA/cm²) at each position. Pipette diameter, 2.5 μm; pipette resistance, 680 kΩ. Shunt resistances were between 1.1 and 1.9 MΩ and there was no correlation between the shunt and the large or small currents. Holding potential, −132 mV. Fiber 1107-6.

mV (mean ± SD), about one-fifth that at the endplate. A plot of Na current densities determined in the region near the endplate from four fibers is shown in Fig. 11. As in the snake, we found the peak Na current density to be very much greater near the endplate than it is away from it. If anything, the density of Na current appears to fall off more steeply with distance in the FDB than it does in the snake. Thus, although the fit was not well constrained, the falling off of density in Fig. 11 is consistent with a length constant of ~30 μm.

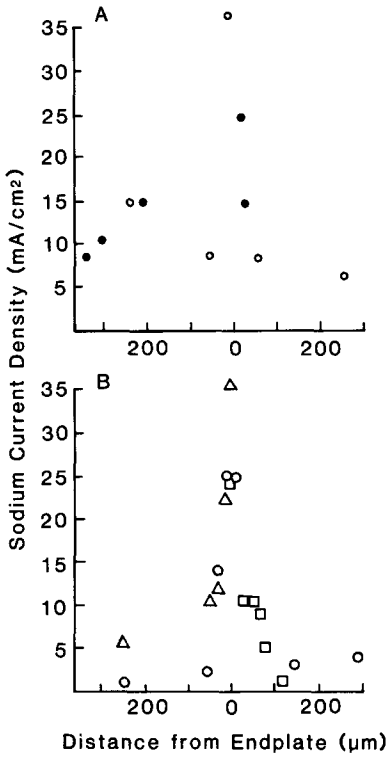

FIGURE 11. Peak inward Na current density as a function of distance from the endplate in rat FDB muscle. (*A*) Fiber 4-24. The open circles were obtained from measurements progressing from left to right and the solid circles were from those progressing from right to left. (*B*) Combined data from three fibers: 15-1 (circles), 18-1 (triangles), and 4-23 (squares). As in Fig. 3, none of the measurements was made from sites overlapping the endplate.

Current density is low near the tendon. Because the fibers of the FDB are very short, it seemed possible that the distribution of Na channels might be different in the longer fibers more typical of mammalian skeletal muscle. We thus used the dissociated omohyoid preparation, in which it was possible to determine the distribution of Na current densities near the endplate, at midfiber locations that were far from both the endplate and the tendon, and also in the region near the tendon. Fig. 12 shows three plots of the peak Na current density determined in dissociated rat omohyoid muscle fibers. In the omohyoid muscle, as in the snake muscle and the rat FDB, the peak Na current density is considerably higher close

to the endplate. Midfiber densities are intermediate in size, and the Na current density falls to low levels near the tendon. Two other dissociated omohyoid fibers that were mapped less completely also showed a marked falling off of peak Na current density near the tendon.

Intact fibers. The reduced current density near the tendon was consistent in all the dissociated omohyoid muscles. These fibers, however, were fragile because of the enzymatic treatment. For a detailed map of the tendon, we returned to the intact omohyoid. As described earlier, visibility in the intact omohyoid did not permit us to map the fiber accurately in the region of the

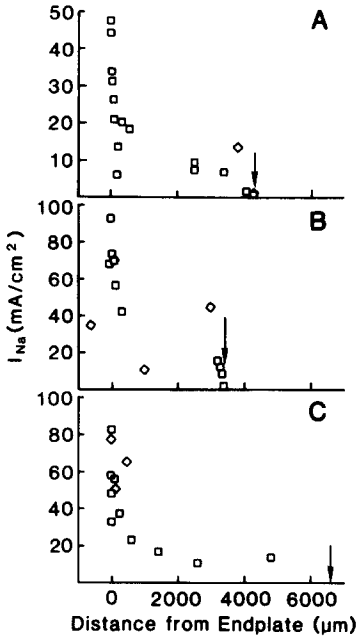

FIGURE 12. Na current densities measured in dissociated rat omohyoid muscle fibers. In all frames, the points represented by the squares were obtained sequentially from left to right and those represented by the diamonds were subsequently obtained from right to left. The arrows indicate the location of the tendons. Fibers 29-1 (*A*), 24-1 (*B*), and 27-1 (*C*).

endplate. However, the omohyoid has a tendon that runs perpendicularly across the center of the muscle, and in this region the fibers are sufficiently ordered so that one can unambiguously follow a single fiber over a considerable distance. Fig. 13 plots Na current densities measured in the region of the tendon in an intact omohyoid muscle fiber. The peak Na current density fell dramatically as the electrode approached the tendon. At a distance of 25 μm from the tendinous termination, the Na current density was only ~6% of the density measured at distances >1 mm. Most of this decrease occurred within 200–300 μm of the tendon. Thus, in both rat and snake muscle, the Na current density is low near the tendon.

As mentioned above, for the endplate region of rat muscle it was possible to map Na currents with the loose patch clamp only with enzymatically dissociated fibers. The increased density of Na channels near the endplate was confirmed in intact muscle using a vibrating microelectrode. The edge of an intact omohyoid muscle with a well-defined, visible endplate band was first scanned with the vibrating electrode. A steady current was found, with an outward peak centered at the endplate band. This current was abolished by replacement of external Cl with isethionate. A similar current in rat lumbrical muscle is created by a nonuniform Cl conductance (Betz et al., 1984*a*). When veratrine (a mixture of veratridine and other alkaloids) was added to the bath to open Na channels, an inward current was induced. This inward current was centered at the endplate band (Fig. 14) and was abolished by TTX (not shown).

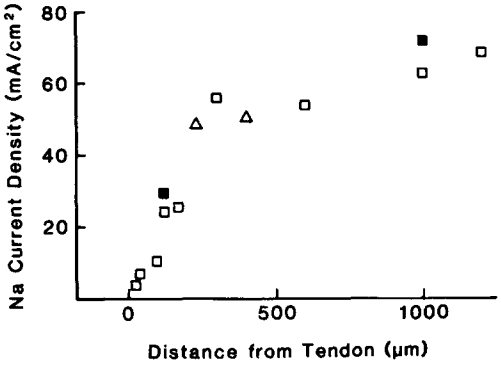

FIGURE 13. Decline of peak inward Na current density near the tendon of an intact rat omohyoid muscle. Points plotted as squares were taken sequentially from right to left; points plotted as triangles were taken subsequently from left to right. The points plotted as solid squares were measured at the same locations as the points immediately below them, but after a longer period at the hyperpolarized holding potential (the lower points of each pair were measured at 2 min; the upper point near 1,000 μm was measured after an additional minute at the holding potential, and the upper point near 125 μm was measured after an additional 2 min). Holding potential, −126 mV. Fiber 34-24.

TTX Sensitivity of Na Channels Near the Endplate

Na-dependent regenerative responses can be measured from the endplate region of both rat (Thesleff et al., 1974) and frog (Nasledov et al., 1982) muscle in the presence of micromolar TTX, which leads to the hypothesis that TTX-insensitive Na channels are located near the endplate. The ability to measure Na currents near the endplate using the loose patch technique permits a direct test of this hypothesis. Such a test is illustrated in Fig. 15*A*, which shows the blocking effect of 250 nM TTX on Na currents measured 15 μm from the endplate of an intact snake muscle fiber. In this fiber, exposure to 250 nM TTX reduced the peak Na current to 7% of the pre-exposure control. After washout of the toxin, the peak current recovered to ~86% of the control value. Fig. 15*B* shows a plot of

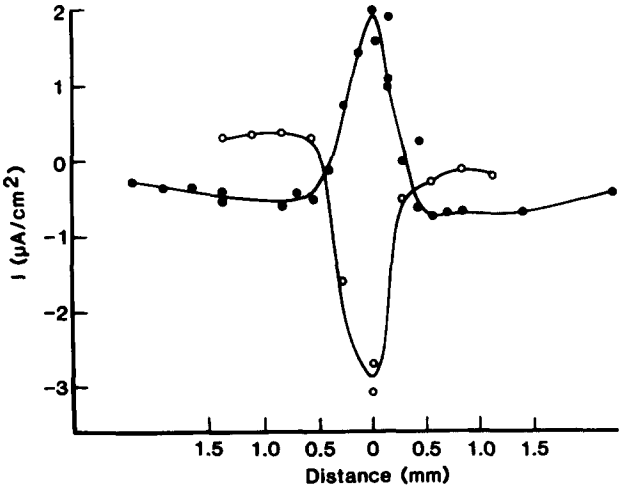

FIGURE 14. Na current measured with a vibrating microelectrode. Intact omohyoid muscle. The positive current on the ordinate is current leaving the muscle. In normal Ringer (solid circles), an endogenous current was present that was outward in the region centered at the endplate band (at position zero on the abscissa). The activation of Na channels by the addition of veratrine (1 mM) resulted in a steady inward current centered at the endplate band (open circles). α-Bungarotoxin was present to block synaptic currents.

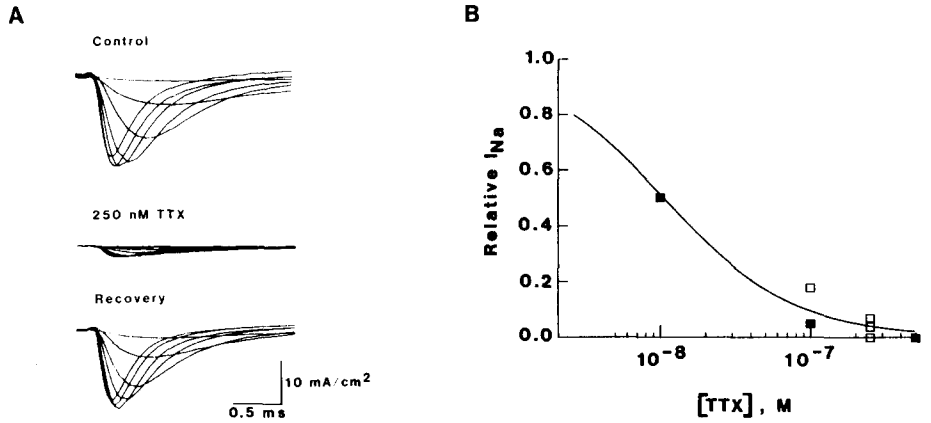

FIGURE 15. TTX block of Na current measured near the endplate in snake muscle fibers. (*A*) Currents measured before, during exposure to, and after a 20-min washout of 250 nM TTX. Recordings were from a single site 15 μm from the endplate of an intact snake muscle fiber. Pipette diameter, 18 μm. Fiber 35-13. Test potentials were from −52.5 to −7.5 mV in 7.5-mV steps. To improve the signal-to-noise ratio, test currents in TTX were signal-averaged four times. (*B*) Dose-response curve for block of Na current. The ordinate gives the ratio of the peak current in the presence of TTX to the peak current at the same site before exposure to TTX. The solid points were determined in a single fiber, and the open symbols in four other fibers. All sites were within 20 μm of the fiber endplate. The smooth curve plots $1/(1 + [\text{TTX}]/K_d)$ with $K_d = 10$ nM.

the ratio of peak Na current in various concentrations of toxin to the pre-toxin control current. The curve represents block of Na current assuming a single dissociation constant of 10 nM for TTX binding to the blocking site. We conclude that if toxin-insensitive channels are present near the endplate of snake muscle, then they must be there at very low density.

DISCUSSION

The loose patch clamp reveals that in vertebrate skeletal muscle fibers, large changes in Na current density occur over distances of several hundred micrometers. Compared with the midfiber region, the most dramatic variations are found under and adjacent to the nerve terminal (where the density is much higher) and near the tendon (where the density is much lower). Although changes in the membrane area under the pipette (discussed in detail below) would affect the measured current, it is doubtful that these are responsible for most of our observations. Variations in channel kinetics or unitary conductance would also affect the measured current density, but again it seems unlikely that these could account for the 100-fold differences we observed. Thus, the simplest interpretation of the changes in measured current density is that they are due to changes in channel density.

Spatial Map of Na Channels

Endplate. The largest currents were recorded when the pipette lay on top of the endplate membrane with the nerve terminal removed (rat dissociated muscle fibers). In most cases, the pipette probably recorded from both synaptic and nonsynaptic membrane because the two are interspersed at mammalian endplates. The extremely high Na current densities recorded directly from the endplate region were calculated assuming that the membrane area was simply the area circumscribed by the pipette mouth and did not include any additional area caused by membrane folding. On the basis of this assumption, the current density of 400 mA/cm^2 would represent the highest density of voltage-gated channels recorded from any tissue. For comparison, vertebrate nodes of Ranvier exhibit maximum Na current densities of 80–100 mA/cm^2; it is estimated that the channel density of large nodes of Ranvier is ~2,000 channels/μm^2 (see Hille, 1984, for a discussion of channel densities in a variety of excitable membrane preparations). If we make the simplest assumption, that channel densities scale with current densities, then 400 mA/cm^2 would represent ~8,000 channels/μm^2. This number is strikingly similar to the 10,000 ACh receptor channels/μm^2 at the top of the junctional folds in vertebrate endplates determined from α-bungarotoxin binding (Fertuck and Salpeter, 1976; Matthews-Bellinger and Salpeter, 1978).

Although the current recorded with large pipettes from the endplate region is severalfold larger than that of near-endplate membrane, the current density related to the amount of sarcolemmal membrane may be about the same: we have not measured the membrane capacitance of the patch, and there could be as much as fivefold more subsynaptic membrane because of secondary folding (Salpeter and Eldefrawi, 1973). However, adding the secondary folds to the membrane area used for normalization assumes that Na channels are distributed

uniformly in the endplate region, which is probably not the case. Using small pipettes, we measured large variations in Na current density at the endplate. The small Na currents (<10 mA/cm^2) might be artifacts, e.g., caused by fragments of nerve or Schwann cell that covered portions of the endplate. Alternatively, some regions of the endplate may lack Na channels.

Regardless of the actual current density, it seems clear that Na channels occur in endplate membrane. They may be located in receptor-free regions, in secondary folds, and possibly even on the tops of the folds among the ACh receptors. On the basis of extracellular recordings of propagating action potentials, Werman (1963) concluded that postsynaptic membrane of frog muscle is inexcitable. In the frog, the synaptic membrane is arranged in elongated ribbons running parallel to the fiber axis (Ishikawa et al., 1983). Thus, in contrast to the rat, it may be possible to record exclusively from subsynaptic membrane of the frog. If Werman's results are correct, they suggest that the small Na currents we observed at the endplate may have been recorded when the pipette was primarily on subsynaptic membrane.

Near the endplate. The density of the Na current adjacent to the endplate is 5–10 times larger than that several hundred micrometers farther from the endplate (Beam et al., 1985*a*; Roberts and Almers, 1985). On the basis of recordings of action potentials (Nastuk and Alexander, 1973), the Na channel density also appears to be increased in the endplate region of frog muscle. It seems very unlikely that differences in the effective area of membrane from which the loose patch pipette records could account for this large difference. Moreover, the capacitance measurements of Roberts and Almers (1985) suggest that the effective membrane area varies little with position along the fiber.

The Na current density decreases with both circumferential and longitudinal distances from the endplate. The decrease with distance appeared to be about the same for both directions. Thus, the current density at the opposite side of the fiber from the endplate (antipode) is normally intermediate between that adjacent to the endplate and that of far extrajunctional regions. We conclude that the focal point of the increased density is the endplate.

Extrajunctional, far from the endplate and tendon. Closely spaced recordings far from the endplate and the tendon of snake muscle showed variations in channel density of as much as two to threefold, similar to those discovered by Almers et al. (1983*a*) in frog muscle. There were no external morphological features that correlated with these variations.

Near the tendon. As the tendon was approached, the current density remained at approximately midfiber levels until the electrode was several hundred micrometers from the end of the fiber. The current density then fell smoothly and rapidly to very low levels at the end of the fiber. It is unlikely that these recordings are complicated by changes in the amount of membrane under the electrode because (*a*) the recordings were not from the extensively folded membrane at the very end of the fiber, and (*b*) using electron microscopy, Eisenberg and Milton (1984) have shown in frog muscle that the amount and proportion of surface and T-system membrane is almost identical near the tendon and in extrajunctional membrane far from the tendon.

Function of the Nonuniform Distribution

One can imagine two reasons why it might be important to have an increased Na channel density near the endplate. First, the presence of extra Na channels would help to overcome the shunting effect created by activated ACh channels (Fatt and Katz, 1951). Second, at regions away from the endplate, the Na channels need only contribute enough current to bring to threshold the region of the fiber ahead of the advancing action potential. At the endplate, the Na channels must supply current to bring fiber regions on both sides of the endplate to threshold. Thus, the increased density of Na channels near the endplate would compensate for this increased electrical load, thereby increasing the safety factor for neuromuscular transmission. An increased safety factor might be particularly important under conditions when neurotransmitter release is depressed (e.g., tetanic stimulation). Even for a single presynaptic action potential, an increased safety factor may be important for some fibers. For example, in some frog twitch muscle fibers, a single presynaptic stimulus releases insufficient neurotransmitter to elicit a twitch (for review, see Grinnell and Herrera, 1981); presumably, conditions that facilitate transmitter release are required for activation. Obviously, for fibers like these, the safety factor would be critical.

The cause of the variations in extrajunctional channel density is not clear. Stühmer and Almers (1982) have shown that Na channels have very low lateral mobility, and Almers et al. (1983*a*) have suggested that the regions of increased density may reflect localized channel insertion. Alternatively, Na channels might aggregate after insertion. Similar mechanisms may operate in axonal membrane. Smith et al. (1982) found that when they experimentally demyelinated axons, localized regions of increased Na current density appeared in the internodal membrane before remyelination. It will be useful to determine whether axons that are normally nonmyelinated have similar variations in Na channel density.

The rapid decrease in Na current density near the tendon seems reasonable from a functional point of view since the end of the fiber behaves as a terminated cable. Thus, passive depolarization is likely to be sufficient to bring this terminated segment rapidly to contraction threshold.

Comparison of Channel Properties Near and Far from the Endplate

Thesleff et al. (1974) and Nasledov et al. (1982) reported that in the presence of TTX, Na-dependent, local, active responses still occurred in the endplate region but not in extrajunctional regions of rat and frog muscle. They therefore proposed that there are Na channels near the endplate that are TTX resistant in normally innervated muscle. We tested this possibility in snake muscle and found no evidence for TTX-resistant channels at the endplate. Preliminary experiments on innervated rat FDB muscle indicate that all Na channels, including those both near and at the endplate, are sensitive to TTX (Caldwell and Milton, 1985). It may be that the local active responses cited above are a consequence of the high density of channels rather than altered TTX sensitivity.

Voltage is not explicitly measured with the loose patch clamp technique and "rim currents" may distort the true kinetics (Almers et al., 1983*a*). Thus, detailed kinetic comparisons of currents from different regions are difficult. Nonetheless,

in both snake and rat muscle, the kinetics of endplate and extrajunctional Na currents showed no obvious differences. Similarly, in snake costocutaneous muscle, Roberts and Almers (1985) found no differences in the kinetics of Na current close to and far from the endplate.

Alternative Techniques for Channel Localization

Hansen Bay and Strichartz (1980) used the binding of tritiated saxitoxin (STX) to study the distribution of Na channels in rat diaphragm. They cut whole muscles into five segments, each of which was several millimeters in length. STX binding of the segments closest to the tendon was 75% of that in the endplate segment. It seems unlikely that this 25% decrease is related to the abrupt decrease of Na current density we observed near the tendon, because their segments were several millimeters in length and the tendons were cut off. The segment containing the endplate band had the same or a lower STX binding as the neighboring extrajunctional segments. A possible explanation for the discrepancy between their results and ours is that the endplate segment contained a substantial amount of extrajunctional membrane, which masked the increase near the endplate. More recent work with fluorescent Na channel toxins demonstrates that Na channels are concentrated near synapses on myotubes in tissue culture (Angelides, 1986). In Angelides' work, the possibility that the increased Na channel density is a consequence of membrane folding was excluded by control experiments with fluorescently labeled lipid or concanavalin A.

Freeze-fracture studies of muscle have revealed nonuniform distributions of membrane proteins. Particles termed "square arrays" are found in higher density in fast muscle and are more numerous away from the endplate than near the endplate (Ellisman et al., 1976). Rogart (1981) speculated that these might be Na channels. The loose patch clamp measurements rule out this possibility since the distribution of Na current density is different from that of the square arrays. The distribution of Na channels reported here will be useful for comparison with other morphological or cytochemical studies.

Fibrillation

Denervated muscle produces spontaneous action potentials called fibrillation potentials, which are used clinically as a diagnosis of denervation. Fibrillation is initiated by oscillatory potential changes or by small rapid depolarizations, both of which are blocked by TTX or by the removal of extracellular Na (Purves and Sakmann, 1974). One curious feature of fibrillation is that the action potentials originate near the denervated endplate (Belmar and Eyzaguirre, 1966; Purves and Sakmann, 1974). If the high density of Na channels near the endplate is maintained in denervated muscle, this might explain the tendency for spontaneous action potentials to originate there.

Control of Channel Distribution

Na channels are not the only channels nonuniformly distributed along the muscle fiber. For many years, only the cholinergic channel was known to have longitudinal variations in density. In addition to being highly concentrated beneath the

nerve terminal, ACh channels are more concentrated in the near-endplate region (Miledi, 1960; Kuffler and Yoshikami, 1975; Bekoff and Betz, 1977) and in some cases in the tendon region (Katz and Miledi, 1964) than in midfiber, extrajunctional membrane. Other channels are also nonuniformly distributed. Inward rectifier K^+ channels appear to be most abundant near the endplate of frog muscle (Katz and Miledi, 1982), whereas the opposite is true for Cl^- channels in rat muscle (Betz et al., 1984*a*). Precise maps of the K^+ and Cl^- channel distributions have not been made and the purpose of these specializations is not understood.

Although the nerve may be ultimately responsible for all these nonuniform distributions, it seems certain that the expression of this control is complex and may not always be direct. The control of ACh receptor distribution has been studied extensively (Fambrough, 1979). There is evidence that muscle activity (Lomo and Rosenthal, 1972), trophic chemical factors (Miledi, 1960), molecules in the basal lamina (McMahan et al., 1980), surface contact (Peng and Cheng, 1982), and steady electric fields (Orida and Poo, 1978) can influence ACh receptor channel localization. The relative importance of these mechanisms for the development and maintenance of the ACh receptor distribution has yet to be determined. Furthermore, the differences in distribution between different channel types imply that no single mechanism will control all of them.

This research was supported by National Institutes of Health grants NS 14901 (K.G.B.) and NS 16922 (J.H.C.), by National Science Foundation grant BNS-8418742 (J.H.C.), by grants from the Muscular Dystrophy Association of America to J.H.C., K.G.B., and D.T.C., and by Research Career Development Award NS 00840 (K.G.B.).

Original version received 8 July 1985 and accepted version received 21 March 1986.

REFERENCES

Almers, W., W. M. Roberts, and R. L. Ruff. 1984. Voltage clamp of rat and human skeletal muscle: measurements with an improved loose-patch technique. *Journal of Physiology.* 347:751–768.

Almers, W., P. R. Stanfield, and W. Stühmer. 1983*a*. Lateral distribution of sodium and potassium channels in frog skeletal muscle: measurements with a patch clamp technique. *Journal of Physiology.* 336:261–284.

Almers, W., P. R. Stanfield, and W. Stühmer. 1983*b*. Slow changes in currents through sodium channels in frog muscle membrane. *Journal of Physiology.* 339:253–271.

Almers, W., and C. Stirling. 1984. Distribution of transport proteins over animal cell membranes. *Journal of Membrane Biology.* 77:169–186.

Angelides, K. J. 1986. Fluorescently labeled Na channels are localized and immobilized to synapses of innervated muscle fibres. *Nature.* In press.

Beam, K. G., J. H. Caldwell, and D. T. Campbell. 1985*a*. Na channels in skeletal muscle concentrated near the neuromuscular junction. *Nature.* 313:588–590.

Beam, K. G., J. H. Caldwell, and D. T. Campbell. 1985*b*. Sodium channels in skeletal muscle are present at higher density near the neuromuscular junction. *Biophysical Journal.* 47:189*a*. (Abstr.)

Bekoff, A., and W. J. Betz. 1977. Physiological properties of dissociated muscle fibers obtained from innervated and denervated adult rat muscle. *Journal of Physiology.* 271:25–40.

Belmar, J., and C. Eyzaguirre. 1966. Pacemaker site of fibrillation potentials in denervated mammalian muscle. *Journal of Neurophysiology.* 29:425–441.

Betz, W. J., and J. H. Caldwell. 1984. Mapping electric currents around skeletal muscle with a vibrating probe. *Journal of General Physiology.* 83:143–156.

Betz, W. J., J. H. Caldwell, and S. C. Kinnamon. 1984*a*. Physiological basis of a steady endogenous current in rat lumbrical muscle. *Journal of General Physiology.* 83:175–192.

Betz, W. J., J. H. Caldwell, and S. C. Kinnamon. 1984*b*. Increased sodium conductance in the synaptic region of rat skeletal muscle fibres. *Journal of Physiology.* 352:189–202.

Brigant, J. L., and A. Mallart. 1982. Presynaptic currents in mouse motor endings. *Journal of Physiology.* 333:619–636.

Caldwell, J. H., and R. L. Milton. 1985. Tetrodotoxin-resistant sodium channels in denervated muscle are concentrated at the neuromuscular junction. *Journal of General Physiology.* 86:15*a*. (Abstr.)

Catterall, W. A. 1981. Localization of sodium channels in cultured neural cells. *Journal of Neuroscience.* 1:777–783.

Chiu, S. Y., and J. M. Ritchie. 1980. Potassium channels in nodal and internodal axonal membrane of mammalian myelinated fibres. *Nature.* 284:170–171.

Conti, F., B. Hille, B. Neumcke, W. Nonner, and R. Stämpfli. 1976. Measurement of the conductance of the sodium channel from current fluctuations at the node of Ranvier. *Journal of Physiology.* 262:699–727.

Eisenberg, B. R., and R. L. Milton. 1984. Muscle fiber termination at the tendon in the frog's sartorius: a stereological study. *American Journal of Anatomy.* 171:273–284.

Ellisman, M. H., J. E. Rash, L. A. Staehelin, and K. R. Porter. 1976. Studies of excitable membranes. II. A comparison of specializations at neuromuscular junctions and non-junctional sarcolemmas of mammalian fast and slow twitch muscle fibers. *Journal of Cell Biology.* 68:752–774.

Fambrough, D. M. 1979. Control of acetylcholine receptors in skeletal muscle. *Physiological Reviews.* 59:165–227.

Fatt, P., and B. Katz. 1951. An analysis of the end-plate potential recorded with an intracellular electrode. *Journal of Physiology.* 115:320–370.

Fertuck, H. C., and M. M. Salpeter. 1974. Localization of acetylcholine receptor by ^{125}I-labeled α-bungarotoxin binding at mouse motor endplates. *Proceedings of the National Academy of Sciences.* 71:1376–1378.

Fishman, H. M. 1975. Patch voltage clamp of squid axon membrane. *Journal of Membrane Biology.* 24:265–277.

Grinnell, A. D., and A. A. Herrera. 1981. Specificity and plasticity of neuromuscular connections: long-term regulation of motoneuron function. *Progress in Neurobiology.* 17:203–282.

Hansen Bay, C. M., and G. R. Strichartz. 1980. Saxitoxin binding to sodium channels of rat skeletal muscles. *Journal of Physiology.* 300:89–103.

Hille, B. 1984. Ionic Channels of Excitable Membranes. Sinauer Associates, Inc., Sunderland, MA. 205–225.

Hille, B., and D. T. Campbell. 1976. An improved vaseline gap voltage clamp for skeletal muscle fibers. *Journal of General Physiology.* 67:265–293.

Ishikawa, H., H. Sawada, and E. Yamada. 1983. Surface and internal morphology of skeletal muscle. *In* The Handbook of Physiology: Skeletal Muscle. L. D. Peachey and R. H. Adrian, editors. American Physiological Society, Bethesda, MD. 1–21.

Jaffe, L. F., and R. Nuccitelli. 1974. An ultrasensitive vibrating probe for measuring steady extracellular currents. *Journal of Cell Biology.* 63:614–628.

Jaimovitch, E., R. A. Venosa, P. Shrager, and P. Horowicz. 1976. Density and distribution of tetrodotoxin receptors in normal and detubulated frog sartorius muscle. *Journal of General Physiology.* 67:399–416.

Katz, B., and R. Miledi. 1964. Further observations on the distribution of acetylcholine-reactive sites in skeletal muscle. *Journal of Physiology.* 170:379–388.

Katz, B., and R. Miledi. 1982. An endplate potential due to potassium released by the motor nerve impulse. *Proceedings of the Royal Society of London B Biological Sciences.* 216:497–507.

Kuffler, S. W., and D. Yoshikami. 1975. The distribution of acetylcholine sensitivity at the post-synaptic membrane of vertebrate skeletal twitch muscles: iontophoretic mapping in the micron range. *Journal of Physiology.* 244:703–730.

Lomo, T., and J. Rosenthal. 1972. Control of ACh sensitivity by muscle activity in the rat. *Journal of Physiology.* 221:493–513.

Matthews-Bellinger, J., and M. M. Salpeter. 1978. Distribution of acetylcholine receptors at frog neuromuscular junctions with a discussion of some physiological implications. *Journal of Physiology.* 279:197–213.

McMahan, U. J., D. R. Edgington, and D. P. Kuffler. 1980. Factors that influence regeneration of the neuromuscular junction. *Journal of Experimental Biology.* 89:31–42.

Miledi, R. 1960. Junctional and extra-junctional acetylcholine receptors in skeletal muscle fibres. *Journal of Physiology.* 151:24–30.

Nasledov, G. A., E. M. Volkov, and G. I. Poletaev. 1982. The effect of tetrodotoxin on the synaptic and extrasynaptic membrane in frog skeletal muscle. *Experientia.* 38:576–577.

Nastuk, W. L., and J. L. Alexander. 1973. Non-homogeneous electrical activity in single muscle fibers. *Federation Proceedings.* 32:333. (Abstr.)

Orida, N., and M.-M. Poo. 1978. Electrophoretic movement and localization of acetylcholine receptors in the embryonic muscle cell membrane. *Nature.* 275:31–35.

Pappone, P. A. 1980. Voltage-clamp experiments in normal and denervated mammalian skeletal muscle fibres. *Journal of Physiology.* 306:377–410.

Peng, H. B., and P.-C. Cheng. 1982. Formation of postsynaptic specializations induced by latex beads in cultured muscle cells. *Journal of Neuroscience.* 2:1760–1774.

Purves, D., and B. Sakmann. 1974. Membrane properties underlying spontaneous activity of denervated muscle fibres. *Journal of Physiology.* 239:125–153.

Ritchie, J. M., and R. B. Rogart. 1977. Density of sodium channels in mammalian myelinated nerve fibers and nature of the axonal membrane under the myelin sheath. *Proceedings of the National Academy of Sciences.* 74:211–215.

Roberts, W. M., and W. Almers. 1985. Increased Na^+ current density near endplates in snake skeletal muscle. *Biophysical Journal.* 47:189*a*. (Abstr.)

Rogart, R. 1981. Sodium channels in nerve and muscle membrane. *Annual Review of Physiology.* 43:711–725.

Salpeter, M. M., and M. E. Eldefrawi. 1973. Sizes of endplate compartments, densities of acetylcholine receptor, and other quantitative aspects of neuromuscular transmission. *Journal of Histochemistry and Cytochemistry.* 21:769–778.

Smith, K. J., H. Bostock, and S. M. Hall. 1982. Saltatory conduction precedes remyelination in axons demyelinated with lysophosphatidyl choline. *Journal of Neurological Science.* 54:13–31.

Strickholm, A. 1961. Impedance of a small electrically isolated area of the muscle cell surface. *Journal of General Physiology.* 44:1073–1088.

Stühmer, W., and W. Almers. 1982. Photobleaching through glass micropipettes: sodium channels without lateral mobility in the sarcolemma of frog skeletal muscle. *Proceedings of*

the National Academy of Sciences. 79:946–950.

Stühmer, W., W. M. Roberts, and W. Almers. 1983. The loose patch clamp. *In* Single-Channel Recording. B. Sakmann and E. Neher, editors. Plenum Press, New York. 123–132.

Thesleff, S., F. Vyskocil, and M. R. Ward. 1974. The action potential in end-plate and extrajunctional regions of rat skeletal muscle. *Acta Physiologica Scandinavica.* 91:196–202.

Werman, R. 1963. Electrical inexcitability of the frog neuromuscular synapse. *Journal of General Physiology.* 46:517–531.